Editors' Suggestion | Featured in Physics

Variational Quantum Monte Carlo Method with a Neural-Network Ansatz for Open Quantum Systems

Alexandra Nagy and Vincenzo Savona
Institute of Physics, Ecole Polytechnique Fédérale de Lausanne (EPFL), CH-1015, Lausanne, Switzerland

(Received 28 February 2019; published 28 June 2019)

The possibility to simulate the properties of many-body open quantum systems with a large number of degrees of freedom (d.o.f.) is the premise to the solution of several outstanding problems in quantum science and quantum information. The challenge posed by this task lies in the complexity of the density matrix increasing exponentially with the system size. Here, we develop a variational method to efficiently simulate the nonequilibrium steady state of Markovian open quantum systems based on variational Monte Carlo methods and on a neural network representation of the density matrix. Thanks to the stochastic reconfiguration scheme, the application of the variational principle is translated into the actual integration of the quantum master equation. We test the effectiveness of the method by modeling the two-dimensional dissipative XYZ spin model on a lattice.

DOI: 10.1103/PhysRevLett.122.250501

Open quantum systems have evolved into a major field of studies in recent years. Focus of these studies are the characterization of emergent phenomena and dissipative phase transitions [1–23], as well as the ongoing debate about whether quantum computing schemes are still hard to simulate classically—and thus achieve quantum supremacy—when in presence of some degree of noise-induced decoherence [24–27].

Assuming a Markovian interaction with the environment, the dynamics of open quantum systems is governed by the quantum master equation in Lindblad form [28]. Only few models within this description admit an analytical solution [29,30]. The quest for efficient numerical methods to simulate the dynamics and the asymptotic steady state resulting from the Lindblad master equation is a research field that is still in its infancy. Many recent tools have been developed following in the footsteps of well-established numerical methods for the simulations of closed, Hamiltonian quantum systems. In particular, matrix-product state and tensor network schemes [31–34], a real-space renormalization approach [35], cluster mean-field [19], and other *ad hoc* approximation schemes [23,36] have recently emerged.

A groundbreaking progress in the numerical simulation of both the ground state and the dynamics of closed quantum systems has recently been made with the introduction of the neural-network variational ansatz [37–43], which efficiently represents highly correlated quantum states and whose parameters are easily optimized by means of the variational Monte Carlo (VMC) method. Recently, a self-adjoint and positive semidefinite parametrization of the density matrix, in terms of a neural network, has been introduced [44].

The steady state of an open quantum system can be characterized by a variational principle [31,33,45,46], whereby the dissipative part of the real-time dynamics, under quite general conditions, drives the system towards a unique steady state in analogy to the imaginary-time Schrödinger equation that leads to the ground state of Hamiltonian systems.

In this Letter, we present a VMC approach to simulate the nonequilibrium steady state (NESS) of open quantum systems governed by the quantum master equation in Lindblad form. The density matrix is parametrized using a neural network ansatz [44] and parameters are varied using an extension of the stochastic reconfiguration method [47], which is shown to approximate the real-time dynamics of the system. We apply the present VMC method to study the steady-state properties of the dissipative XYZ spin model [19–23] that displays a prototypical second-order dissipative phase transition. Thanks to the Monte Carlo sampling of expectation values, this method holds promise for the efficient simulation of open quantum systems with a large number of d.o.f.

Dynamics of open quantum systems.—The dynamics of the density matrix $\hat{\rho}$ of an open quantum system is governed by the quantum master equation which—in case of Markovian coupling to the environment—takes the Lindblad form

$$\frac{d\hat{\rho}}{dt} = -i[\hat{H},\hat{\rho}] - \sum_i \frac{\gamma_i}{2}[\{\hat{F}_i^\dagger \hat{F}_i,\hat{\rho}\} - 2\hat{F}_i\hat{\rho}\hat{F}_i^\dagger], \quad (1)$$

where the curly brackets denote the anticommutator. The unitary part of the dynamics is generated by the term depending on the Hamiltonian $\hat{H}$, while $\hat{F}_i$ are the jump

operators associated to the dissipative processes induced by the environment. The equation is typically expressed in terms of the Liouvillian superoperator as $d\hat{\rho}/dt = \mathcal{L}(\hat{\rho})$, whose formal solution is $\hat{\rho}(t) = e^{\mathcal{L}t}\hat{\rho}(0)$ $(t > 0)$. The existence and uniqueness of a NESS—defined as $\hat{\rho}_{\mathrm{SS}} = \lim_{t\to\infty}\hat{\rho}(t)$—satisfying

$$\mathcal{L}(\hat{\rho}_{\mathrm{SS}}) = 0 \tag{2}$$

has been demonstrated under quite general assumptions [48,49], in particular for finite-size spin and boson lattices [48].

The steady state can be computed as the long-time limit of the solution of the quantum master equation, or by directly solving the homogeneous linear system [Eq. (2)] with an additional condition on the trace of the density matrix. In both cases, the size of the problem is quantified by the square of the Hilbert space dimension, thus becoming computationally prohibitive already for a modest number of d.o.f. A promising route to the numerical computation of the NESS is provided by the variational principle. In cases where a unique steady state exists [48], the NESS corresponds to the eigenmatrix of the Liouvillian superoperator $\mathcal{L}$ with a zero eigenvalue [49]. As all other eigenvalues have a strictly negative real part, the NESS can be formally derived as the matrix that maximizes the real part of the expectation value (computed in matrix space) of the Liouvillian.

Neural network density matrix.—We assume that the Hilbert space of the system is spanned by the computational basis $|\boldsymbol{\sigma}\rangle$, where $\boldsymbol{\sigma} = (\sigma_1, \sigma_2, \ldots, \sigma_N)$ labels the states of N d.o.f. that compose the system. Here and in what follows we will assume binary local d.o.f, with $\sigma_i = \{-1, 1\}$, which applies to the broad class of interacting spin-1/2 or qubit models. The density matrix in this basis is formally expressed as $\rho(\boldsymbol{\sigma}, \boldsymbol{\eta}) = \langle\boldsymbol{\sigma}|\hat{\rho}|\boldsymbol{\eta}\rangle$ in terms of the density operator $\hat{\rho}$. We denote a specific variational ansatz for the density matrix as $\rho_\chi(\boldsymbol{\sigma}, \boldsymbol{\eta})$, where $\chi = (\chi_1, \chi_2, \ldots, \chi_{N_p})$ is a set of variational parameters.

A neural network ansatz for a self-adjoint, positive semidefinite density matrix was recently introduced [44] in the specific form of a restricted Boltzmann machine (RBM). In a variational approach, RBMs present the significant advantage that the sum over the hidden-spin configurations can be carried out analytically, and the logarithmic derivatives with respect to the variational parameters admit simple expressions [39]. Here we briefly describe how this ansatz can be derived from simple considerations on the density matrix. A self-adjoint, positive, semidefinite expression for the density matrix is

$$\rho_\chi(\boldsymbol{\sigma}, \boldsymbol{\eta}) = \sum_{j=1}^{J} p_j(\chi)\psi_j(\boldsymbol{\sigma}, \chi)\psi_j^*(\boldsymbol{\eta}, \chi). \tag{3}$$

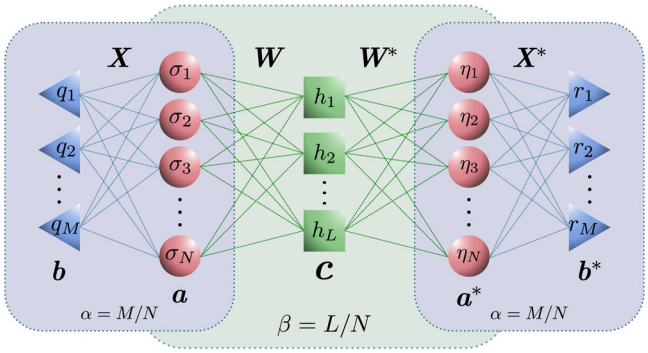

FIG. 1. Graphical representation of the neural network ansatz for the density matrix. The input states $|\boldsymbol{\sigma}\rangle, |\boldsymbol{\eta}\rangle$ are encoded in the visible layer, represented by circles. The hidden spins in the triangles encode the correlation between the physical spins in each state of the statistical mixture, while the hidden spins in the squares encode the mixture between the states. This structure is easily seen to coincide with a RBM, where the hidden layer is composed by the triangle and square nodes.

The states $\psi_j(\boldsymbol{\sigma}, \chi)$ are not necessarily mutually orthogonal and the sum extends over J states, with $J \leq d$ and $d = 2^N$ being the dimension of the Hilbert space under study.

We start by introducing a RBM ansatz for each state $\psi_j(\boldsymbol{\sigma}, \chi)$ entering Eq. (3). A RBM is composed of two layers of binary valued nodes (see Fig. 1): a visible layer for encoding the physical state and a hidden layer. Each node is associated with a bias (a and b parameters) and nodes in the different layers are connected via a set of weighted edges (X parameters). For a large number of hidden nodes, this structure is known to describe quantum correlations efficiently [38,41].

In order to express the mixed structure in Eq. (3) as a single RBM, we embed an intermediate set of L hidden nodes that are used to express the probabilities $p_j(\chi)$ in RBM form as $p_j(\chi) = \exp(\sum_l c_l h_l)$, with $h_l = \pm 1$ and $c_l \in \mathbb{R}$. To index the different states in the mixture accordingly, this new set of hidden nodes must also enter the RBM expression of the wave functions. When carrying out the sums over configurations of hidden nodes, the final expression for the RBM density matrix is [50]

$$\begin{aligned}\rho_\chi(\boldsymbol{\sigma}, \boldsymbol{\eta}) = 8 \exp\left(\sum_i a_i\sigma_i\right) \exp\left(\sum_i a_i^*\eta_i\right) \\ \times \prod_{l=1}^{L} \cosh\left(c_l + \sum_i W_{li}\sigma_i + \sum_i W_{li}^*\eta_i\right) \\ \times \prod_{m=1}^{M} \cosh\left(b_m + \sum_i X_{mi}\sigma_i\right) \\ \times \prod_{n=1}^{M} \cosh\left(b_n^* + \sum_i X_{ni}^*\eta_i\right).\end{aligned} \tag{4}$$

The RBM is sketched in Fig. 1, and $\chi = \{a_i, b_m, X_{mi}, c_l, W_{li}\}$ is the final set of parameters, which

are assumed as complex valued with the exception of c_l that must take real values. The representational power of the RBM is determined by the number of hidden nodes [54]. Here we set the densities of hidden nodes through the parameters $\alpha = M/N$, $\beta = L/N$, which measure the representational power of the RBM ansatz independently of the size of the spin lattice. When separately accounting for the real and imaginary parts of complex-valued parameters, the total number of computational parameters in the RBM ansatz is $N_p = N[(\alpha+\beta)(2N+1)+\alpha+2]$. In what follows, we will always assume $\alpha = \beta$ for simplicity.

Optimization.—It is convenient to rewrite Eq. (2) in a vectorized form by reshaping $\hat{\rho}$ into a column vector $|\rho\rangle$. Following [45], $\mathcal{L}$ takes matrix form and the steady state density matrix fulfills $\langle\rho|\mathcal{L}|\rho\rangle = 0$. Therefore the expectation value over the variational density matrix $\langle\!\langle \mathcal{L}_\chi \rangle\!\rangle = \langle\rho_\chi|\mathcal{L}|\rho_\chi\rangle / \langle\rho_\chi|\rho_\chi\rangle$ is a function of the variational parameters χ. The parameter values that best approximate $\langle\!\langle \mathcal{L}_\chi \rangle\!\rangle = 0$ can be found by means of various optimization procedures [39,42,44,55]. In this Letter, we choose to adopt the stochastic reconfiguration (SR) scheme by Sorella *et al.* [47], which we extend to open quantum systems. The parameters are initialized to a small random value and, at each iteration, they are updated as

$$\chi(n+1) = \chi(n) + \nu S^{-1}(n) F(n), \tag{5}$$

where the learning rate ν is small enough to guarantee convergence. It can be shown [50] that the SR scheme induces, at each iteration, a variation in the parameters that best approximates the time evolution of the density matrix over a time step ν. Here, we define the covariance matrix S, the vector of forces F, and the logarithmic derivatives O as

$$\begin{aligned} O_k(\boldsymbol{\sigma},\boldsymbol{\eta}) &= \frac{1}{\rho_\chi(\boldsymbol{\sigma},\boldsymbol{\eta})} \frac{\partial \rho_\chi(\boldsymbol{\sigma},\boldsymbol{\eta})}{\partial \chi_k}, \\ F_k(n) &= \langle\!\langle O_k^* \mathcal{L} \rangle\!\rangle - \langle\!\langle \mathcal{L} \rangle\!\rangle \langle\!\langle O_k^* \rangle\!\rangle, \\ S_{kk'}(n) &= \langle\!\langle O_k^* O_{k'} \rangle\!\rangle - \langle\!\langle O_k^* \rangle\!\rangle \langle\!\langle O_{k'} \rangle\!\rangle, \end{aligned} \tag{6}$$

where $k, k' = 1, 2, \ldots, N_p$. The notation $\langle\!\langle \cdot \rangle\!\rangle$ denotes the normalized expectation value taken over the variational density matrix $|\rho_\chi\rangle$, and the derivatives $O_k(\boldsymbol{\sigma},\boldsymbol{\eta})$ are taken as diagonal operators in these expectation values. We point out that, while the expression for S in Eq. (6) results in the VMC iterations following the real time evolution, minimization can be achieved by using any positive-definite covariance matrix. In particular, setting S as the identity results in the steepest descent procedure. Since S can be noninvertible, we apply an explicit regularization scheme as introduced in Ref. [39]: $S^{\mathrm{reg}}_{kk'} = S_{kk'} + \lambda(n)\delta_{k,k'}S_{kk'}$, where $\lambda(n) = \max(\lambda_0 b^n, \lambda_{\min})$. For the present calculations, they were set to $\lambda_0 = 100$, $b = 0.998$, and $\lambda_{\min} = 10^{-2}$.

Sampling.—The various expectation values in Eq. (6) must be evaluated at each iteration step. We evaluate these quantities stochastically over a Markov-chain of N_{MH} configurations $(\boldsymbol{\sigma},\boldsymbol{\eta})$ sampling the square modulus of the density matrix $|\rho_\chi(\boldsymbol{\sigma},\boldsymbol{\eta})|^2$. For this we adopt the Metropolis-Hastings algorithm [53]. In the limit of $N_{\mathrm{MH}} \to \infty$, the statistical error decays as $1/\sqrt{N_{\mathrm{MH}}}$. Choosing an appropriate set of rules for the random walk is key to an efficient Monte Carlo sampling. Here we randomly choose each move among those allowed by the Liouvillian superoperator [50].

Observables.—Once the optimal parameter values have been determined, the expectation value of any quantum mechanical observable $\hat{\mathcal{O}}$ over the steady state can be expressed as

$$\langle\hat{\mathcal{O}}\rangle = \mathrm{Tr}(\hat{\mathcal{O}}\hat{\rho}_\chi) = \sum_{\boldsymbol{\sigma},\boldsymbol{\eta}} |\rho_\chi(\boldsymbol{\sigma},\boldsymbol{\eta})|^2 \frac{\mathcal{O}(\boldsymbol{\eta},\boldsymbol{\sigma})}{\rho_\chi(\boldsymbol{\sigma},\boldsymbol{\eta})^*}, \tag{7}$$

which can also be evaluated using the Metropolis-Hastings algorithm. For all the quantities considered here, the expectation values were additionally averaged over 100 sets of parameter values $\chi(n)$ chosen in the asymptotic region of the SR interation in order to improve the statistical accuracy. The overall error in the sampled observables has, in addition to the contribution from the Metropolis-Hastings algorithms, a contribution from the SR scheme and a systematic contribution related to the representational power of the RBM ansatz, as measured by the α and β parameters.

Computational cost.—The number of floating point operations to evaluate Eq. (6) scales as N_p^3, if we assume that the number of Metropolis-Hastings steps N_{MH} is set to roughly the number of parameters N_p, as in Ref. [39]. The Metropolis-Hastings procedure also scales with the number of connected states N_c, i.e., with the average number of nonzero elements in a column of the Liouvillian matrix. Finally, the efficiency of the whole procedure thus scales as $O(N_p^3 + N_p N_c)$.

Results.—To assess the effectiveness of the method, we study a spin-1/2 XYZ model on a two-dimensional lattice with periodic boundary condition. Each spin is subject to a dissipation process into the $|\sigma^z = -1\rangle$ state. This model has been already widely investigated and is known to display a dissipative phase transition between a paramegnetic and a ferromagnetic phase [19–23]. The Hamiltonian and the quantum master equation read ($\hbar = 1$)

$$\hat{H} = \sum_{\langle i,j \rangle} (J_x \hat{\sigma}_i^x \hat{\sigma}_j^x + J_y \hat{\sigma}_i^y \hat{\sigma}_j^y + J_z \hat{\sigma}_i^z \hat{\sigma}_j^z), \tag{8}$$

$$\frac{d\hat{\rho}}{dt} = -i[\hat{H},\hat{\rho}] - \frac{\gamma}{2}\sum_k [\{\hat{\sigma}_k^+ \hat{\sigma}_k^-, \hat{\rho}\} - 2\hat{\sigma}_k^- \hat{\rho} \hat{\sigma}_k^+], \tag{9}$$

where $\hat{\sigma}_j^x$, $\hat{\sigma}_j^y$, $\hat{\sigma}_j^z$ are the Pauli matrices, $\hat{\sigma}_j^{\pm} = (\hat{\sigma}_j^x \pm i\hat{\sigma}_j^y)/2$, J_α are the coupling constants between nearest neighbor spins, and γ is the dissipation rate. The excitations in the system—induced by the anisotropic spin coupling—compete with the isotropic dissipative process, and this competition is at the origin of the dissipative phase transition [19–23]. The effectiveness of the neural network ansatz is demonstrated by studying the system observables across a phase boundary.

In addition to the expectation value $\langle\langle \mathcal{L}_\chi \rangle\rangle$, we study the local magnetization

$$M_z = \frac{1}{N}\sum_{i=1}^{N} \mathrm{Tr}(\hat{\rho}\hat{\sigma}_i^z), \tag{10}$$

and the steady state structure factor

$$S_{\mathrm{SS}}^{xx}(\mathbf{k}) = \frac{1}{N(N-1)}\sum_{\mathbf{j}\neq\mathbf{l}} e^{-i\mathbf{k}\cdot(\mathbf{j}-\mathbf{l})}\langle\hat{\sigma}_{\mathbf{j}}^x\hat{\sigma}_{\mathbf{l}}^x\rangle, \tag{11}$$

computed for the asymptotic steady state.

Figure 2 shows the convergence of $S_{\mathrm{SS}}^{xx}(\mathbf{k}=\mathbf{0})$ and $S_{\mathrm{SS}}^{xx}(\mathbf{k}=(2\pi/3,0))$ to the exact result for a 3×3 lattice, as

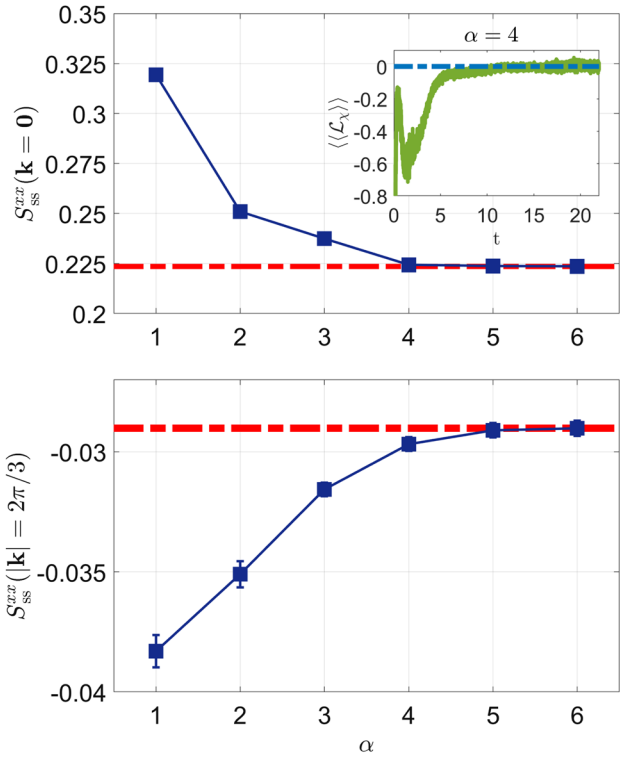

FIG. 2. The steady state spin structure factor $S_{\mathrm{SS}}^{xx}(\boldsymbol{k})$ computed as a function of $\alpha=\beta$ for a 3×3 lattice and $\mathbf{k}=\mathbf{0}$ (upper panel) and $\mathbf{k}=(2\pi/3,0)$ (lower panel). The red dot-dashed line represents in both panels the exact result. The inset shows the evolution of $\langle\langle \mathcal{L}_\chi \rangle\rangle$ over the VMC run. Parameters: $J_x/\gamma = 0.9$, $J_y/\gamma = 1.2$, $J_z/\gamma = 1.0$.

$\alpha=\beta$ are increased. The parameters χ are initialized randomly and updated at each VMC step according to the SR scheme [50]. The parameters of the model are chosen to lie in the vicinity of the dissipative phase transition, i.e., $J_x/\gamma = 0.9$, $J_y/\gamma = 1.2$, $J_z/\gamma = 1.0$. A clear convergence towards the exact value upon increasing $\alpha=\beta$ is found. The inset in Fig. 2 shows the SR evolution of $\mathrm{Re}(\langle\langle \mathcal{L}_\chi \rangle\rangle)$ over a typical VMC run. The oscillations at early times are a feature of the unitary part of the dynamics in the quantum master equation.

In Fig. 3 we display the magnetization as computed for different lattice sizes and as a function of the coupling parameter J_y/γ. For this choice of parameters, a para-to-ferromagnetic phase transition is expected to occur when increasing the coupling through the value $J_y \gtrapprox 1.04$ [21,22], while a second phase boundary between a ferromagnetic and a paramagnetic region has been predicted by cluster mean-field calculations at around $J_y \gtrapprox 1.4$. For 2×2 and 3×3 lattices, the VMC result agrees well with the exact calculation for a large enough number of variational parameters.

In Fig. 4 we display the spin structure factor $S_{\mathrm{SS}}^{xx}(\mathbf{k}=\mathbf{0})$ for the same parameters as in Fig. 3. The quantity $S_{\mathrm{SS}}^{xx}(\mathbf{k}=\mathbf{0})$ vanishes when in a paramagnetic phase, while it takes a finite value in the ferromagnetic region of the phase diagram. This behavior is displayed both by the exact calculation for small lattices, and by the VMC data, in the vicinity of the phase boundary at $J_y \gtrapprox 1.04$. For values $J_y > 1.4$ the system should become again paramagnetic in the thermodynamic limit of large lattices, but this feature was not displayed by the present data up to the largest

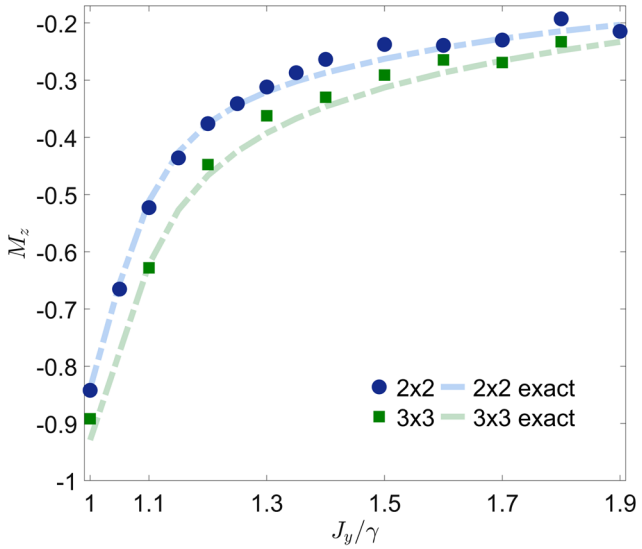

FIG. 3. The magnetization M_z computed as a function of the coupling J_y/γ. VMC and exact values are compared. Error bars, when not shown, are smaller than the symbol. Other parameters: $J_x/\gamma = 0.9$, $J_z/\gamma = 1.0$, $\alpha=\beta=3$.

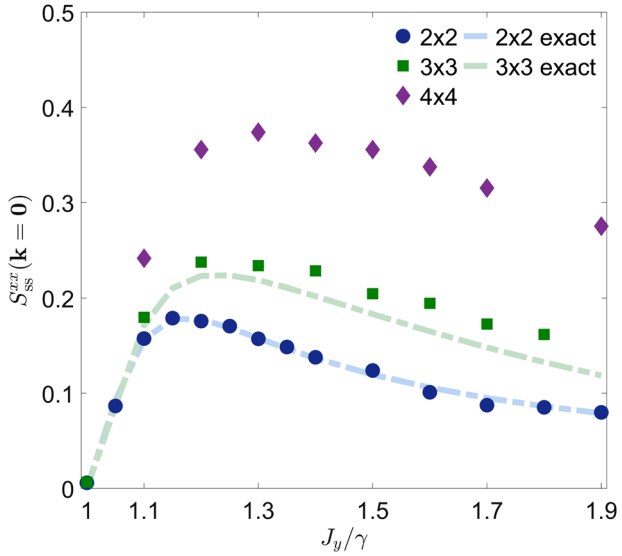

FIG. 4. The steady-state spin structure factor $S^{xx}_{ss}(\mathbf{k}=\mathbf{0})$ computed as a function of the coupling J_y/γ. VMC and exact values are compared. Other parameters: $J_x/\gamma = 0.9, J_z/\gamma = 1.0, \alpha = \beta = 3$.

lattice under study, in agreement also with recent stochastic Gutzwiller calculations [23].

In all the calculations, special care was devoted to the choice of the SR time step ν. The unitary part of the real-time dynamics generated by Eq. (1) makes the differential equation stiff, thus requiring to scale down ν appropriately as the system size—and thus the spectral width of the differential operator—is increased. A possible workaround would be to study an effective, purely dissipative dynamics using the superoperator $\mathcal{L}^\dagger\mathcal{L}$ as a generator. In the case of a unique steady state, this superoperator is self-adjoint and positive semidefined, with the only null eigenvalue being associated to the steady-state solution. We argue that this effective dynamics would be more robust to the choice of the time step. The superoperator $\mathcal{L}^\dagger\mathcal{L}$ is however less sparse than $\mathcal{L}$ on the computational basis, calling for an efficient sampling scheme.

Existing numerical approaches to the simulation of the steady state of a Markovian open quantum system either require the full representation of the Hilbert space into memory, or rely on a properly chosen truncation of the Hilbert space to a relevant subspace. The present VMC approach is free of these two limitations, thanks to the stochastic evaluation of expectation values by means of the Metropolis-Hastings algorithm. The neural network ansatz in terms of a RBM is highly representative of quantum correlated statistical mixtures, while being simple to handle numerically. In cases with very strong quantum correlations, this ansatz could be extended to deep network representations, as was recently done in the case of Hamiltonian problems [37,38,43,56]. For some of these networks [56], the hidden d.o.f. can still be summed analytically, as for RBMs. Neural network representations are not restricted to spin d.o.f. and have been successfully adopted to represent bosonic many-body states efficiently [57]. For these reasons, the present VMC approach may emerge as the election tool to numerically model open quantum systems, with considerable impact on the study of fundamental physics and on the modeling of near-term, noisy quantum information platforms [27].

We are indebted to Giuseppe Carleo and Markus Holzmann for enlightening discussions. The work was supported by the Swiss National Science Foundation through Project No. 200021_162357 and 200020_185015.

Note added.—While developing the present result, we became aware of three related independent works that have been carried out in parallel [58–60].

[1] I. Carusotto and C. Ciuti, Rev. Mod. Phys. **85**, 299 (2013).
[2] M. J. Hartmann, J. Opt. **18**, 104005 (2016).
[3] C. Noh and D. G. Angelakis, Rep. Prog. Phys. **80**, 016401 (2017).
[4] N. Bartolo, F. Minganti, W. Casteels, and C. Ciuti, Phys. Rev. A **94**, 033841 (2016).
[5] A. Biella, F. Storme, J. Lebreuilly, D. Rossini, R. Fazio, I. Carusotto, and C. Ciuti, Phys. Rev. A **96**, 023839 (2017).
[6] M. Biondi, G. Blatter, H. E. Türeci, and S. Schmidt, Phys. Rev. A **96**, 043809 (2017).
[7] H. J. Carmichael, Phys. Rev. X **5**, 031028 (2015).
[8] W. Casteels, R. Fazio, and C. Ciuti, Phys. Rev. A **95**, 012128 (2017).
[9] W. Casteels, F. Storme, A. Le Boité, and C. Ciuti, Phys. Rev. A **93**, 033824 (2016).
[10] J. M. Fink, A. Dombi, A. Vukics, A. Wallraff, and P. Domokos, Phys. Rev. X **7**, 011012 (2017).
[11] T. Fink, A. Schade, S. Höfling, C. Schneider, and A. Imamoglu, Nat. Phys. **14**, 365 (2018).
[12] M. Fitzpatrick, N. M. Sundaresan, A. C. Y. Li, J. Koch, and A. A. Houck, Phys. Rev. X **7**, 011016 (2017).
[13] M. Foss-Feig, P. Niroula, J. T. Young, M. Hafezi, A. V. Gorshkov, R. M. Wilson, and M. F. Maghrebi, Phys. Rev. A **95**, 043826 (2017).
[14] E. M. Kessler, G. Giedke, A. Imamoglu, S. F. Yelin, M. D. Lukin, and J. I. Cirac, Phys. Rev. A **86**, 012116 (2012).
[15] J. Marino and S. Diehl, Phys. Rev. Lett. **116**, 070407 (2016).
[16] V. Savona, Phys. Rev. A **96**, 033826 (2017).
[17] L. M. Sieberer, S. D. Huber, E. Altman, and S. Diehl, Phys. Rev. Lett. **110**, 195301 (2013).
[18] F. Vicentini, F. Minganti, R. Rota, G. Orso, and C. Ciuti, Phys. Rev. A **97**, 013853 (2018).
[19] J. Jin, A. Biella, O. Viyuela, L. Mazza, J. Keeling, R. Fazio, and D. Rossini, Phys. Rev. X **6**, 031011 (2016).
[20] T. E. Lee, S. Gopalakrishnan, and M. D. Lukin, Phys. Rev. Lett. **110**, 257204 (2013).
[21] R. Rota, F. Minganti, A. Biella, and C. Ciuti, New J. Phys. **20**, 045003 (2018).
[22] R. Rota, F. Storme, N. Bartolo, R. Fazio, and C. Ciuti, Phys. Rev. B **95**, 134431 (2017).

[23] W. Casteels, R. M. Wilson, and M. Wouters, Phys. Rev. A **97**, 062107 (2018).
[24] M. J. Bremner, A. Montanaro, and D. J. Shepherd, Quantum **1**, 8 (2016).
[25] X. Gao and L. Duan,arXiv:1810.03176.
[26] A. W. Harrow and A. Montanaro, Nature (London) **549**, 203 (2017).
[27] J. Preskill, Quantum **2**, 79 (2018).
[28] H.-P. Breuer and F. F. Petruccione, *The Theory of Open Quantum Systems* (Oxford University Press, New York, 2002), p. 625.
[29] T. Prosen, Phys. Rev. Lett. **107**, 137201 (2011).
[30] T. Prosen, Phys. Rev. Lett. **112**, 030603 (2014).
[31] J. Cui, J. I. Cirac, and M. C. Bañuls, Phys. Rev. Lett. **114**, 220601 (2015).
[32] A. Kshetrimayum, H. Weimer, and R. Orús, Nat. Commun. **8**, 1291 (2017).
[33] E. Mascarenhas, H. Flayac, and V. Savona, Phys. Rev. A **92**, 022116 (2015).
[34] A. H. Werner, D. Jaschke, P. Silvi, M. Kliesch, T. Calarco, J. Eisert, and S. Montangero, Phys. Rev. Lett. **116**, 237201 (2016).
[35] S. Finazzi, A. Le Boité, F. Storme, A. Baksic, and C. Ciuti, Phys. Rev. Lett. **115**, 080604 (2015).
[36] A. Nagy and V. Savona, Phys. Rev. A **97**, 052129 (2018).
[37] Z. Cai and J. Liu, Phys. Rev. B **97**, 035116 (2018).
[38] G. Carleo, Y. Nomura, and M. Imada, Nat. Commun. **9**, 5322 (2018).
[39] G. Carleo and M. Troyer, Science **355**, 602 (2017).
[40] N. Freitas, G. Morigi, and V. Dunjko, Int. J. Quantum. Inform. **16**, 1840008 (2018).
[41] I. Glasser, N. Pancotti, M. August, I. D. Rodriguez, and J. I. Cirac, Phys. Rev. X **8**, 011006 (2018).
[42] Y. Nomura, A. S. Darmawan, Y. Yamaji, and M. Imada, Phys. Rev. B **96**, 205152 (2017).
[43] X. Gao and L.-M. Duan, Nat. Commun. **8**, 662 (2017).
[44] G. Torlai and R. G. Melko, Phys. Rev. Lett. **120**, 240503 (2018).
[45] M. Jakob and S. Stenholm, Phys. Rev. A **67**, 032111 (2003).
[46] H. Weimer, Phys. Rev. Lett. **114**, 040402 (2015).
[47] S. Sorella, M. Casula, and D. Rocca, J. Chem. Phys. **127**, 014105 (2007).
[48] D. Nigro, arXiv:1803.06279.
[49] F. Minganti, A. Biella, N. Bartolo, and C. Ciuti, Phys. Rev. A **98**, 042118 (2018).
[50] See Supplemental Material at http://link.aps.org/supplemental/10.1103/PhysRevLett.122.250501 for more information on the neural network ansatz, the stochastic reconfiguration method, the stochastic sampling procedure, and the details of the numerical approach, which includes Refs. [39,47,51–53].
[51] S. Choi, C. Paige, and M. Saunders, SIAM J. Sci. Comput. **33**, 1810 (2011).
[52] Y. Liu, Contribute to syangliu/MINRES-QLP development by creating an account on GitHub (2019), https://github.com/syangliu/MINRES-QLP.
[53] N. Metropolis, A. W. Rosenbluth, M. N. Rosenbluth, A. H. Teller, and E. Teller, J. Chem. Phys. **21**, 1087 (1953).
[54] N. Le Roux and Y. Bengio, Neural Comput. **20**, 1631 (2008).
[55] G. Torlai, G. Mazzola, J. Carrasquilla, M. Troyer, R. Melko, and G. Carleo, Nat. Phys. **14**, 447 (2018).
[56] K. Choo, G. Carleo, N. Regnault, and T. Neupert, Phys. Rev. Lett. **121**, 167204 (2018).
[57] H. Saito, J. Phys. Soc. Jpn. **86**, 093001 (2017).
[58] M. J. Hartmann and G. Carleo, following Letter, Phys. Rev. Lett. **122**, 250502 (2019).
[59] F. Vicentini, A. Biella, N. Regnault, and C. Ciuti, this issue, Phys. Rev. Lett. **122**, 250503 (2019).
[60] N. Yoshioka and R. Hamazaki, Phys. Rev. B **99**, 214306 (2019).